2023 IEEE International Conference on Robotics and Automation (ICRA 2023)
May 29 - June 2, 2023. London, UK

ADAPT: A 3 Degrees of Freedom Reconfigurable Force Balanced Parallel Manipulator for Aerial Applications

Kartik Suryavanshi[1], Salua Hamaza[2], Volkert van der Wijk[1] and Just Herder[1]

***Abstract*—In this paper, we present the ADAPT, a novel reconfigurable force-balanced parallel manipulator for spatial motions and interaction capabilities underneath a drone. The reconfigurable aspect allows different motion-based 3-DoF operation modes like translational, rotational, planar, and so on, without the need for disassembly. For the purpose of this study, the manipulator is used in translation mode only. A kinematic model is developed and validated for the manipulator. The design and motion capabilities are also validated both by conducting dynamics simulations of a simplified model on MSC ADAMS, and experiments on the physical setup.**

The force-balanced nature of this novel design decouples the motion of the manipulator's end-effector from the base, zeroing the reaction forces, making this design ideally suited for aerial manipulation applications, or generic floating-base applications.

***Index Terms*—reactionless force balancing, configurable robot, mechanism design, parallel robot, aerial manipulation.**

I. Introduction

In recent years, there has been increasing interest and effort toward the development of Unmanned Aerial Vehicles (UAVs) with manipulation capabilities to be used for civilian purposes. The energy sector has heavily funded research for the development of UAVs that can monitor and inspect physical infrastructure, respond to natural disasters and help with smart cropping for higher yields in the agricultural and meteorological domains [1]. In the EU, several projects with large consortia further developed mechatronic and software solutions to advance the field of aerial manipulation for industrial inspection and maintenance (I&M). To do this, the UAV has to not only do contact-less tasks like surveillance, monitoring, and remote sensing, but also it has to do active tasks like grasping and manipulation [3].

Interest in aerial manipulation has been steadily growing to their exceptional capabilities when combining the versatility of aerial platforms and the manipulation capabilities of robotic arms. However, there are still many research problems to be solved before aerial manipulators can be put to use. One of the major problems is the complex control of the combination of a drone and a manipulator. There are two ways to develop the motion controller for the combined system [4].

[1] Department of Precision & Microsystems Engineering, Faculty of Mechanical Engineering, TU Delft, the Netherlands. Corresponding author: suryavanshikartik@gmail.com

[2] BioMorphic Intelligence Lab, Department of Control & Operations, Faculty of Aerospace Engineering, TU Delft, the Netherlands.

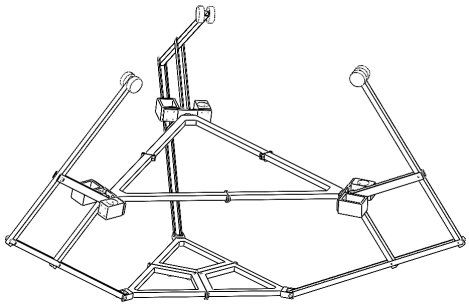

Fig. 1. Wire-frame CAD model of the novel three-legged forced-balanced parallel manipulator. Each leg is composed of an inherently forced-balanced pantograph mechanism. Three legs in parallel link the two bases via a set of revolute joints.

The first approach is to consider the manipulators and the aerial vehicle as two separate entities which have to be controlled independently, i.e. *decentralised* approach. Generally, the manipulators in this approach are considered to be very lightweight and relatively underactuated, such that they do not have a great impact on the dynamics of the aerial vehicle [5]. The decentralised approach is popular in the aerial robotics community, it allows a faster implementation on the two subsystems through decoupling, omitting the need for a full multi-body dynamic model. However, this approach fails when the motion becomes too demanding in terms of accelerations involved, resulting in large tracking errors.

The second approach is to create a dynamic model, such that the UAV and manipulator combination become a single entity [6]. The inertia matrix in this approach consists of coupling terms such that the manipulator and aircraft both affect each other. Having a complete coupled dynamic model leads to the system having better performance in terms of positioning and stability. However, since the system relies on a complete dynamic model, the controller becomes rather complex [7]–[9]. Secondly, model-based controllers assume that torque feedback at the actuator is available, however this is not always the case, especially on lightweight manipulators.

Extensive research in aerial manipulation is conducted in making the controllers better. Conversely, not a lot of thought has been put into improving the manipulator mechanical design such that the dynamical model itself becomes simpler. Removing the coupling between the two subsystems can ease the controller, as the UAV only perceives the manipulator as

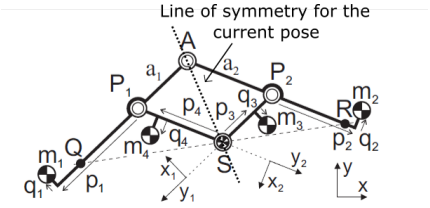

Fig. 2. General 2-DoF pantograph structure with the centre of mass at point S. The pantograph is mass symmetric about the instantaneous line joining points A and S. Since the legs are mass symmetric, the q's have a value of zero and the pantograph can further be simplified. Picture credit [10].

an additional static mass that does not affect the aircraft's dynamics.

In this paper, we propose a new balanced manipulator that does not create any reaction forces during its motion throughout its configuration space. This force-balanced design is such that the center of mass of the manipulator remains fixed. Therefore, there are no coupling mass terms in the complete inertia matrix in the dynamic model of the complete system. This design would make the controller much simpler such that the aerial vehicle still manages to do highly dynamic maneuvers, even with an integrated manipulator.

II. Manipulator Design

One way to create force-balanced spatial manipulators is by designing a structure composed of multiple spatial force-balanced elements as legs such that there is spatial force balancing in individual legs themselves as well as the whole mechanism. This leads to heavier leg designs as a spatially balanced leg requires more balancing elements involving a more complex structure [10]. Another way to create a balanced mechanism is to take 2D planar force-balanced elements and combine them to create a spatial 3D mechanism. The legs are combined in such a way that the addition of moment/force constraint wrenches span the full three dimensions. In other words, the moment/force constraints should be independent, such that they form a basis in three dimensions. The latter method is used to create a spatially force-balanced mechanism in this work since it leads to a design that uses fewer elements for balancing and is less complex.

This spatial forced balanced mechanism is designed in a manner such that it is composed of the pantograph as its legs. A pantograph is a 2-DoF mechanism [10], that is symmetric about the center point 'S' as illustrated in Fig. 2. This symmetry allows the construction of mass symmetric mechanisms which is a precursor to force-balanced mechanisms. The constraint imposed by each leg form a constraint wrench of a pure moment, reciprocal to all the 'R' joints. The moment constraint wrench spans the 3D space, allowing translation in 3D space for the platform (Fig. 3). The three constraints would remain independent unless they reach singularity as defined in Section IV.

Van der Wijk formulated the force balance conditions for pantographs using the linear momentum equations which led to following four conditions to have the CoM fixed at S, and therefore be forced balanced at S.

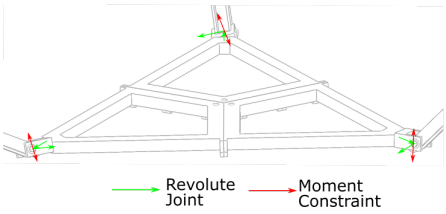

Fig. 3. The constraint wrench in a parallel manipulator is the sum of all the constraint from all the legs. The constraint moment from an individual leg is perpendicular to all the revolute joints.The revolute joints are shown in green colour and constraint moments in red. The sum of these moment constraints span the full 3D space such that the reciprocal freedom screw shows all three translations for the platform.

$$\begin{aligned} m_1 p_1 &= m_2 a_1 + m_3 p_3 \\ m_1 q_1 &= m_3 q_3 \\ m_2 p_2 &= m_1 a_2 + m_4 p_4 \\ m_2 q_2 &= m_4 q_4 \end{aligned} \tag{1}$$

Since the legs are mass symmetric, the values of $q_{1,2,3,4}$ become zero, reducing the system to two equations in two variables, hence fully solvable.

$$\begin{aligned} m_1 p_1 &= m_2 a_1 + m_3 p_3 \\ m_2 p_2 &= m_1 a_2 + m_4 p_4 \end{aligned} \tag{2}$$

Our novel architecture is generated by creating 3 intersecting planes for the robot's legs, equispaced at 120°. On each plane lays a pantograph mechanism. The overall CoM of the assembly is depicted as CoM_t in Fig. 4(a) - this point also remains invariant for any motion of the platform. The invariant CoMs (Ss) of the three pantographs are joined together to the fixed base via universal joints. The lower half of the pantographs (SP_1Q_1) are joined together to a moving platform via 3 universal joints spaced at 120 degrees. The upper half of the pantographs(SP_2Q_2) is free to move. Combining the legs in this way makes the manipulator force balanced. This can be seen by dividing the platform mass equally between the three legs such that each leg is a simple force-balanced pantograph (Fig. 4)

Similarities of the kinematic chain used for the ADAPT robot could be found in the Double-Y 3-5R parallel mechanism (DYMO) seen in Fig. 5 presented by Zlatanov et. al. [17].

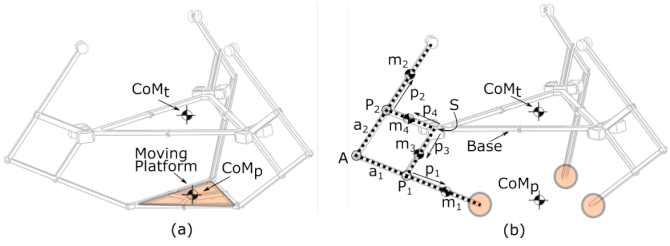

Fig. 4. (a) Actual Setup (b) Equivalent model. The manipulator with the platform mass in (a) is equivalent to the sum of the three m2 (Fig. 2) masses in (b). The base center of mass, CoM_t, is invariant for any motion induced at the end-effector. The tri-symmetric design allows the center of mass of the platform CoM_p to be in the same position in the equivalent model as it were in the actual model.

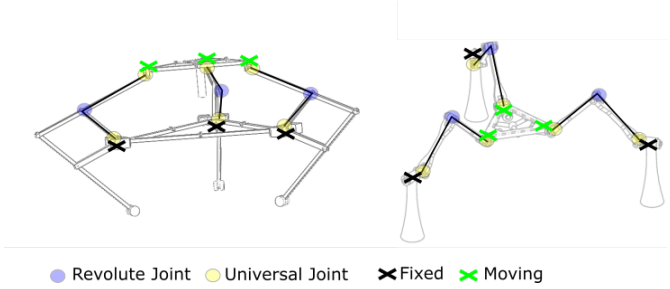

Fig. 5. The similarities in the kinematic chain on the legs of the ADAPT manipulator (left) and the DYMO manipulator (right).

The DYMO robot has five fundamentally different operation modes: translation, rotation, mixed (rotation+ translation), planar, and no motion at all. The translation mode is utilized in the current work to find a forced balanced alternative to the Delta robot. This was done since the Delta robot motion capabilities are predominantly exploited for various applications. While the mechanism is supposed to only translate, the mechanism can also show mixed motions under certain circumstances.

III. Kinematics

A. Forward Kinematics

ADAPT consists of a fixed base connected to a moving platform (end-effector) by three parallel kinematic chains as its legs, as depicted in Fig. 6. Each leg has several passive joints and one active joint centred at each pantograph's CoM, placed symmetrically with respect to the pantograph's legs. This design makes the ADAPT robot different from conventional parallel manipulators where the active joint features as the first joint, at the base.

The motion in ADAPT is transmitted to the moving platform by the lower portion of the pantograph (SP_1Q_1). Moreover, unlike a generic Delta robot, the intermediate leg joint is a revolute and not a universal. There is a 2-DoF relative motion within the Delta robot's leg, contrasting with the 1-DoF relative motion in ADAPT.

The schematic in Fig. 6 shows the kinematic parameters of one of the legs where we just consider the lower portion of the pantograph. The motion of the upper portion (SP_2Q_2), Fig. 4) of the leg is symmetric to the motion of the lower portion.

O represents the center of the fixed platform, while P is the center of the moving platform. The first Cartesian coordinate frame is XYZ which is fixed to the point O. The next reference frame is $X_o\ Y_o\ Z_o$ which has the same XY plane but the frame is rotated about the Z-axis by angle θ_i, which is constant and i is the number of the leg i =1,2,3. The frame $X_o\ Y_o\ Z_o$ has its X-axis towards the attachment point of the leg. r_A and r_B are the radii of the two platforms. Each leg is intended to constrain one rotation such that the platform is only allowed translations when the three legs are attached. So the moving platform is always horizontal. The first revolute joint (the passive joint next to point O is the first joint, the active joint is the second joint, and so on) rotates the complete

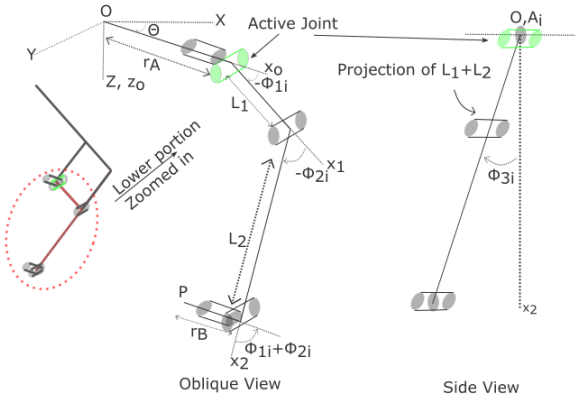

Fig. 6. Schematic diagram of the lower portion of one of the legs with the kinematic parameters. The ϕ_{3i} angle rotates the full leg (Side View) unlike the Delta robot where only the upper link of the leg moves relative to the lower leg. There is 2DoF relative motion within a Delta robot leg contrasting with the 1DoF relative motion in the current leg.

leg about its X-axis. This angle is denoted by ϕ_{3i}. The angle between the first link and the base is denoted by ϕ_{1i}. The angle between the first link and the second link is denoted by ϕ_{2i}. Since the platform is constrained to remain horizontal the magnitude of the fourth angle (fourth revolute from the top) is equal to the sum of the magnitudes of the second and the third angles but with a negative sign. This implicit definition makes kinematics easier to formulate since the number of variables is reduced. Similarly, the magnitude of the last joint angle is equal to and opposite to the magnitude of the first joint angle ($-\phi_{3i}$). L_1 and L_2 are the link lengths as shown in the figure.

To locate the position of point P of the moving platform Denavit-Hartenberg transformation matrices are defined. The sequence of matrix multiplication results in the transformation from the base frame to the platform frame.

$$T_{r_p} = T_{r_Z} T_{t_{ra}} T_{r_{xo}} T_{r_{yo}} T_{t_{L1}} T_{r_{y1}} T_{t_{L2}} T_{r_{y2}} T_{r_{x2}} T_{t_{rb}} T_{r_{Z2}} \quad (3)$$

The resultant matrix is quite large to reproduce here, hence for brevity only the 3 elements from the top right corner have been extracted, denoting the end-effector coordinates.

$$\begin{aligned}
x_{EE} &= \mathrm{r_A}\, C\Theta_\mathrm{i} - \mathrm{r_B}\, C\Theta_\mathrm{i} + L_1\, C\phi_{11}\, C\Theta_\mathrm{i} \\
&\quad + L_2\, C\phi_{11}\, C\phi_{21}\, C\Theta_\mathrm{i} - L_2\, C\Theta_\mathrm{i}\, S\phi_{11}\, S\phi_{21} \\
&\quad - L_1\, S\phi_{11}\, S\phi_{31}\, S\Theta_\mathrm{i} - L_2\, C\phi_{11}\, S\phi_{21}\, S\phi_{31}\, S\Theta_\mathrm{i} \\
&\quad - L_2\, C\phi_{21}\, S\phi_{11}\, S\phi_{31}\, S\Theta_\mathrm{i} \\
y_{EE} &= \mathrm{r_A}\, S\Theta_\mathrm{i} - \mathrm{r_B}\, S\Theta_\mathrm{i} + L_1\, C\phi_{11}\, S\Theta_\mathrm{i} \\
&\quad + L_2\, C\phi_{11}\, C\phi_{21}\, S\Theta_\mathrm{i} + L_1\, C\Theta_\mathrm{i}\, S\phi_{11}\, S\phi_{31} \\
&\quad - L_2\, S\phi_{11}\, S\phi_{21}\, S\Theta_\mathrm{i} + L_2\, C\phi_{11}\, C\Theta_\mathrm{i}\, S\phi_{21}\, S\phi_{31} \\
&\quad + L_2\, C\phi_{21}\, C\Theta_\mathrm{i}\, S\phi_{11}\, S\phi_{31} \\
z_{EE} &= C\phi_{31}\, L_2\, S\phi_{11} + \phi_{21} + L_1\, S\phi_{11}
\end{aligned} \quad (4)$$

Where $S()$ and $C()$ are used for sin and cos functions respectively for brevity. In the complete transformation matrix, the rotation matrix is a constant.

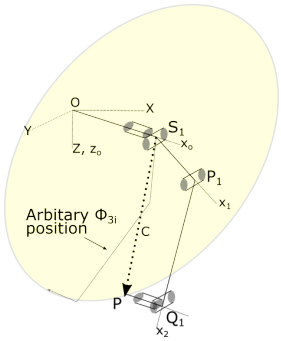

Fig. 7. Schematic diagram of one of the legs with the kinematic parameters.When all the joints are kept fixed and only ϕ_{3i} is allowed to move then the leg endpoint forms a circle with a fixed radius. This radius (C) is independent of the joint variable ϕ_{3i}

B. Inverse Kinematics

Researchers usually find the inverse kinematic Jacobian by getting rid of passive joint variables from the kinematic equations by taking the scalar product such that only the active input variables remain. [12]–[14]. In the current case, the active revolute joints are ϕ_{1i}; i=1,2,3, and all the rest of the revolute joints are passive. Since the active joint comes after the passive joint, ϕ_{3i}, the same trick cannot be applied since the velocity equations are still dependent on the passive variables. We have three equations for the x, y, and z positions of the center of the platform which is composed of three variables ϕ_{11}, ϕ_{21}, and ϕ_{31}. Unlike the previous works, it is not possible to analytically solve all three equations simultaneously therefore geometrical reductions are done to get a relation between two variables.

It can be seen in the figure that the magnitude of the vector OP does not depend on the passive variable ϕ_{31}. The leg ($S_1P_1Q_1P$ in Fig. 7) forms a circle with radius C as can be seen in the figure in yellow. We can calculate the length of the vector OP by squaring and adding the x,y, and z position equations in the transformation matrix. Doing that we see that the dependence on ϕ_{3i} indeed falls off and we can get a relation between ϕ_{2i} and ϕ_{1i}.This is an important geometrical step for reduction. Through further analytical reductions we can find the relation of ϕ_{1i} in terms of the known position variables p_x p_y and p_z.
Once the equation is derived in terms of ϕ_{11}, the Jacobian can be evaluated to find the platform velocity with respect to the time derivative of ϕ_{1i}. The relation between platform velocity (v) and input velocity ($\dot{\theta}$) can be represented in the following form

$$J_p * v = J_\theta * \dot{\theta} \tag{5}$$

It is found that J_θ is a diagonal matrix which implies that the input velocities are independent of each other when moving the platform, which is similar to a conventional Delta robot. Whereas, J_p is a full matrix indicating that the velocity along all three axes is affected by a single input, again similar to a conventional Delta robot.

Fig. 8. CAD model of the current manipulator transitioning from translation mode to mixed freedom mode. As the center moves away from the center's vertical axis the tilt angle increases.

IV. Constraint Singularities

Besides the conventional singularities, the ADAPT manipulator also experiences *constraint singularities*, i.e. singular configurations that may allow transitions between dramatically different operation modes. This type of singularities are also found in the the DYMO robot [1]. One of the operation modes has been exploited in the development of the current manipulator translational capabilities. As suggested in the DYMO paper, for the manipulator to remain parallel and work in the translational mode, the following singularity conditions should be avoided.
i) P $\in O_z$; meaning that the platform center is on the z-axis of the base platform.
ii) Platform plane and the base plane coincide.
iii) A combination of i) and ii) meaning P and O coincide

Condition (ii) and (iii) cannot occur in the physical robot so they can be overlooked. If in case the manipulator is in the singularity condition (i), the platform has to remain parallel to the base plane to remain in the translation mode. The platform can leave the translation mode and get into an undesired mixed freedom mode operation through the constraint singularity, that is when the P $\in O_z$. Results of the *constraint singularities* analysis are presented in Fig. 8.

V. Dynamic Simulation

Dynamic simulations were performed on the multi-body dynamics simulation software MSC ADAMS to validate that the design was forced-balanced. In the software, a simplified model of ADAPT was created where the two links in the leg were replaced by a single one, while preserving the geometry,

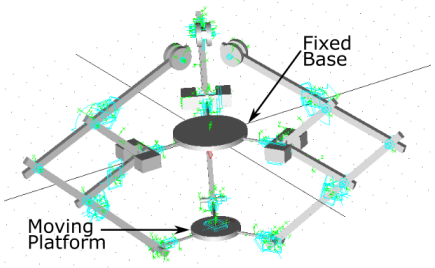

Fig. 9. The ADAPT manipulator model used for dynamic simulations.

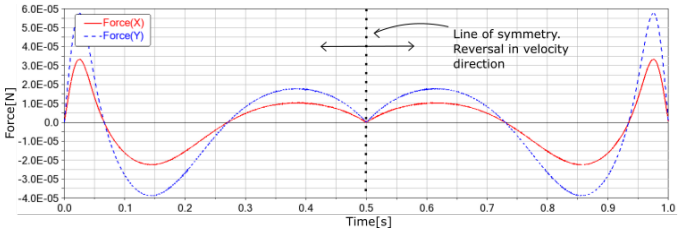

Fig. 10. Reaction forces in the X and the Y direction at the base for straight line traversal of the balanced manipulator platform

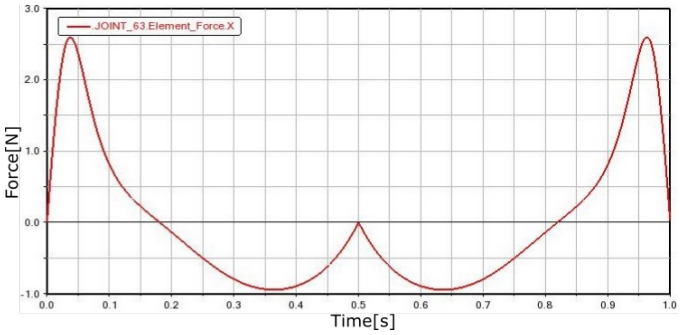

Fig. 11. Reaction forces in the X and the Y direction at the base for straight-line traversal of the unbalanced manipulator platform.

mass and inertia values. In the model, the leg links are also allowed to intersect and maintain the same motion range as in the real setup.

In simulation, the base is fixed and the platform is allowed to move. Joints are modelled as passive. The reaction forces were evaluated at the fixed base joint in the X and Y directions. A step angular input was given to the first leg to traverse in the X direction and then come back to the origin.

The reaction forces measured are in the order of 10^{-5} N, therefore negligible. These negligible errors appear as a result of the numerical nature of this analysis, producing round off errors, discretization errors, and truncation errors. The unbalanced case was also simulated, where the counter-masses of the mechanism were made massless. Results are seen in Figures 10 and 11. In the unbalanced case, the platform goes down under gravity, unlike in the balanced case. When the same simulation was run, it was seen that the platform does not remain horizontal and starts to tilt. Overall, results show that forces are predominantly higher in the unbalanced case.

VI. Fabrication

The starting point in the fabrication was the selection of motors to drive each of the legs independently. As the ADAPT robot is intrinsically force-balanced and and each leg is mass symmetric, motors chosen to actuate the robot do not require a high torque value. In fact, motors only need to work against friction, for which small actuators were favoured. Based on the torque required to drive an unbalanced leg derived from further motion simulations in SolidWorks, smart servos Dynamixel XL430-W250-T were selected. Standard aluminum

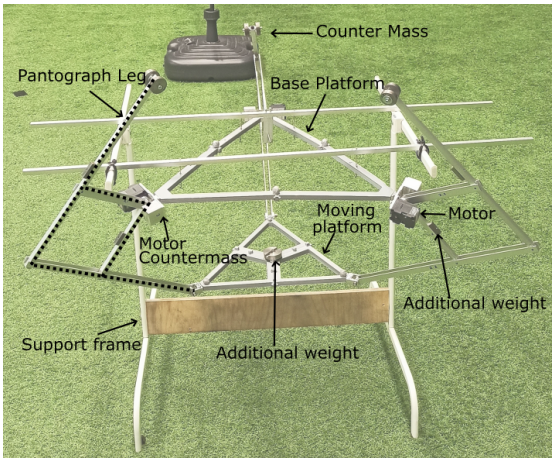

Fig. 12. Experimental Setup of the reactionless manipulator. Additional weight has been added to the links so that the links with equal lengths (but different cross-sections) have equal masses. The additional mass has also been added to the platform so that the total moving mass of the platform is equal to the sum of the masses of the counterweight.

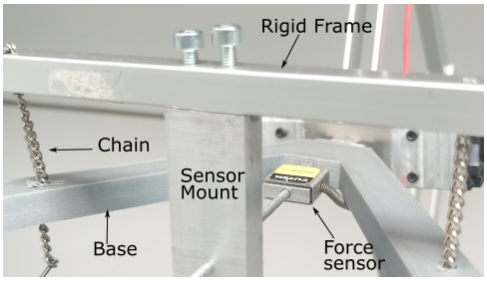

Fig. 13. Experimental setup showcasing the force sensor placement.

plates were used as links. The lengths and masses of the links were defined according to Eq. 1.

The masses of the generic motors and their counter weights resulted in the total weight of the setup to be around 1.9Kg. A triangular design of the moving platform was selected that was tri-symmetrical which allowed equivalent division of the platform mass to the three legs. The platform mass was made equal to the sum of the three m_2 masses to fulfill the balance conditions Eq 1. Moreover, counter-masses were machined in steel so they occupy less volumetric space.

To control the motors, the Arduino UNO micro-controller was used, paired with additional shield to fulfill the servo's communication protocols. Control of the motors was done simultaneously. The inverse kinematics was solved off-board on a dekstop computer running Matlab; then joint angles values were communicated to the motor boards operating in position mode.

Using the FUTEK LSB bi-directional load cell, force values were measured in the X direction using. The load cell is connected to the National Instruments Multi-function I/O acquisition board, with a LabVIEW user-interface to log the data stream.

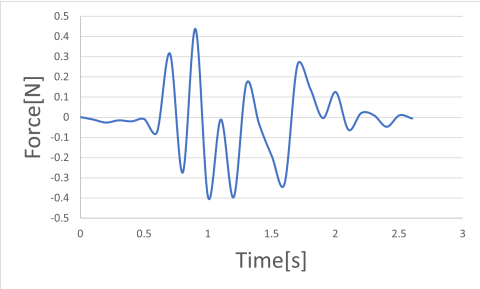

Fig. 14. Reaction force for unbalanced manipulator in the X direction for the experiment when the platform is moved up such that $\phi_{1i} = 40°, i \in 1, 2, 3$, from its resting position (lowest potential)

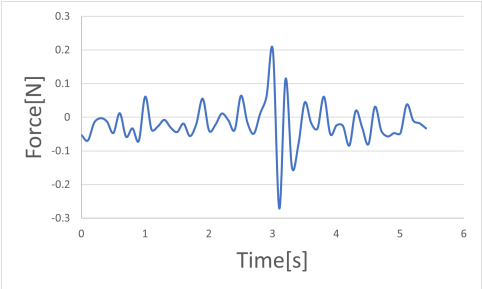

Fig. 16. Reaction forces in the case of an balanced manipulator in the X direction for the experiment when the platform is moved forward and back in the X direction. The motion is such $\phi_{11} = 40°$ in the middle of the cycle.

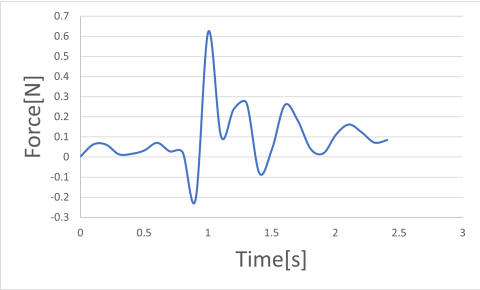

Fig. 15. Reaction forces in the case of an unbalanced manipulator in the X direction for the experiment when the platform is moved forward and back in the X direction. The motion is such $\phi_{11} = 40°$ in the middle of the cycle.

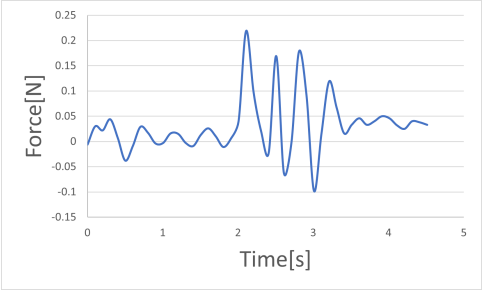

Fig. 17. Reaction force for balanced manipulator in the X direction for the experiment when the platform is moved up such that $\phi_{1i} = 40°, i \in 1, 2, 3$, from the same posiiton as the resting position of the unbalanced case

VII. Experiments

A. Unbalanced Mode

Here, the counter masses displayed in Fig. 12 were removed to emulate the behavior of a generic unbalanced 3-leg parallel manipulator. A step input was given to the first leg to traverse in the X direction and then come back to the origin. Unlike the simulation where no damping or stiction are modeled, stiction present in the real joints worsened translation along the X direction.

Rather the platform tilted more and so lower force values were recorded ($\approx$ .4N). Since the first experiment was not satisfactory a second experiment was conducted. In this experiment, the platform was raised such that, $\phi_{1i} = 40°$. Executing this trajectory, we see that the maximum reaction force generated is ($\approx$ 0.6N). Although these forces are parasitic since the force sensor is mounted in the X direction and the motion is in the Z direction, a comparison can be made with the balanced case since the platform remains horizontal.

B. Balanced Mode

In the balanced case, the counter masses are put back and the first experiment is conducted again. We see some peaks in the resulting plot. These peaks are because the manufactured parts do not have a tight tolerance which leads to backlash therefore when the links are moved, they start and stop with a jerk. However, the forces are still low, $\approx$ 0.5N.

In the second experiment, to imitate the starting conditions of the unbalanced situation, the platform is put to the lowest position manually. From there, again the platform is raised such that $\phi_{1i} = 40°$. We see that the maximum reaction force generated in the X direction is $\approx$ 0.2 N.

There is an offset in the steady state values in both cases after the trajectory is complete. It can be attributed to the way the force sensor is fixed to the base. There is a single thread screw screwed into the metal insert in the 3D printed base. This loose connection allows the metal screw to settle at a different inclined angle and thus not measure exact zero at the steady state in both the cases, as seen in Figures 14, 17.

VIII. Conclusion

In this work, the ADAPT robot is introduced, a force-balanced re-configurable spatial manipulator for aerial robotics applications. The design is capable of different operation modes, while being force balanced in its configuration space. The position kinematics of the manipulator are formulated for the translation mode of operation, the Jacobian matrix is also derived. Constraint singularities for ADAPT are analysed in the configuration space. To validate the force reactionless behavior, simulations are conducted that confirm the expected behavior. A prototype of ADAPT is built to substantiate the results of the simulation. Results show that the measured reaction forces are still substantially lower in the balanced case (less than 50%). Further improvements on the fabrication process can further alleviate minor force errors via the use of tighter tolerances on the joints.

REFERENCES

[1] Amazon Prime Air, 2016. [Online]. Available: http://www.amazon.com/b?node=8037720011

[2] AEROARMS Project, 2014. [Online]. Available: https://cordis.europa.eu/project/id/644271

[3] Ruggiero, Fabio, Vincenzo Lippiello, and Anibal Ollero. "Aerial manipulation: A literature review." IEEE Robotics and Automation Letters 3.3 (2018): 1957-1964.

[4] Ollero, Anibal, et al. "Past, present, and future of aerial robotic manipulators." IEEE Transactions on Robotics 38.1 (2021): 626-645.

[5] Bellicoso, Carmine Dario, et al. "Design, modeling and control of a 5-DoF light-weight robot arm for aerial manipulation." 2015 23rd Mediterranean Conference on Control and Automation (MED). IEEE, 2015.

[6] Suarez, Alejandro, et al. "Design of a lightweight dual arm system for aerial manipulation." Mechatronics 50 (2018): 30-44.

[7] Yang, Hyunsoo, and Dongjun Lee. "Dynamics and control of quadrotor with robotic manipulator." 2014 IEEE international conference on robotics and automation (ICRA). IEEE, 2014.

[8] Yüksel, Burak, Gabriele Buondonno, and Antonio Franchi. "Differential flatness and control of protocentric aerial manipulators with any number of arms and mixed rigid-/elastic-joints." 2016 IEEE/RSJ International Conference on Intelligent Robots and Systems (IROS). IEEE, 2016.

[9] Mersha, Abeje Yenehun, Stefano Stramigioli, and Raffaella Carloni. "On bilateral teleoperation of aerial robots." IEEE Transactions on Robotics 30.1 (2013): 258-274.

[10] Van der Wijk, V. "Methodology for analysis and synthesis of inherently force and momentbalanced mechanisms-theory and applications (dissertation)." University of Twente (free download: http://dx. doi. org/10.3990/1.9789036536301) (2014).

[11] Wijk, V., and Justus Laurens Herder. "Dynamic balancing of Clavel's Delta robot." Computational kinematics. Springer, Berlin, Heidelberg, 2009. 315-322.

[12] López, M., et al. "Delta robot: inverse, direct, and intermediate Jacobians." Proceedings of the Institution of Mechanical Engineers, Part C: Journal of Mechanical Engineering Science 220.1 (2006): 103-109.

[13] Li, Yangmin, and Qingsong Xu. "Kinematic analysis and design of a new 3-DOF translational parallel manipulator." (2006): 729-737.

[14] Tsai, Lung-Wen. Robot analysis: the mechanics of serial and parallel manipulators. John Wiley and Sons, 1999.

[15] Zlatanov, Dimiter, Ilian A. Bonev, and Clément M. Gosselin. "Constraint singularities of parallel mechanisms." Proceedings 2002 IEEE International Conference on Robotics and Automation (Cat. No. 02CH37292). Vol. 1. IEEE, 2002.

[16] Mahmoodi, Mostafa, Mahmood Ghafouri Tabrizi, and Khalil Alipour. "A new approach for Kinematics-based design of 3-RRR delta robots with a specified workspace." 2015 AI and Robotics (IRANOPEN). IEEE, 2015

[17] Zlatanov, D., Bonev, I.A., and Gosselin, C.M., "Constraint Singularities as C-Space Singularities," 8th International Symposium on Advances in Robot Kinematics (ARK 2002), Caldes de Malavella, Spain, June 24–28, 2002.

[18] Patel, Ketankumar H., et al. "Workspace and singularity analysis of 3-RRR planar parallel manipulator." Proceedings of the 1st international and 16th national conference on machines and mechanisms. 2013.